

Fast finite difference solvers for singular solutions of the elliptic Monge-Ampère equation

B. D. Froese^a, A. M. Oberman^{a,*}

^a*Department of Mathematics, Simon Fraser University
Burnaby, British Columbia, Canada, V5A 1S6*

Abstract

The elliptic Monge-Ampère equation is a fully nonlinear Partial Differential Equation which originated in geometric surface theory, and has been applied in dynamic meteorology, elasticity, geometric optics, image processing and image registration. Solutions can be singular, in which case standard numerical approaches fail.

In this article we build a finite difference solver for the Monge-Ampère equation, which converges even for singular solutions. Regularity results are used to select *a priori* between a stable, provably convergent monotone discretization and an accurate finite difference discretization in different regions of the computational domain. This allows singular solutions to be computed using a stable method, and regular solutions to be computed more accurately. The resulting nonlinear equations are then solved by Newton's method.

Computational results in two and three dimensions validate the claims of accuracy and solution speed. A computational example is presented which demonstrates the necessity of the use of the monotone scheme near singularities.

Keywords: Fully Nonlinear Elliptic Partial Differential Equations, Monge Ampère equations, Nonlinear Finite Difference Methods, Viscosity Solutions, Monotone Schemes, Convexity Constraints

1. Introduction

In this article we build a finite difference solver for the Monge-Ampère equation, which converges even for singular solutions. Regularity results are used to select *a priori* between two discretizations in different regions of the computational domain. Near possible singularities, a stable, provably convergent monotone discretization is used. Elsewhere a more accurate discretization is used. This allows singular solutions to be computed using a stable method, and regular solutions to be computed more accurately. The resulting nonlinear equations are then solved by Newton's method, which is fast, $\mathcal{O}(M^{1.3})$, where M is the number of data points, independent of the regularity of the solution.

*Corresponding Author

Email addresses: bdf1@sfu.ca (B. D. Froese), aoberman@sfu.ca (A. M. Oberman)

URL: <http://www.divbyzero.ca/froese/> (B. D. Froese), <http://math.sfu.ca/~aoberman> (A. M. Oberman)

Preprint submitted to Elsevier

February 23, 2024

10 *1.1. The setting for equation*

11 The Monge-Ampère equation is a fully nonlinear Partial Differential Equation (PDE).

$$12 \det(D^2u(x)) = f(x), \quad \text{for } x \text{ in } \Omega. \quad (\text{MA})$$

13 The Monge-Ampère operator, $\det(D^2u)$, is the determinant of the Hessian of the function
14 u . The equation is augmented by the convexity constraint

$$u \text{ is convex}, \quad (\text{C})$$

15 which is necessary for the equation to be elliptic. The convexity constraint is made
16 explicit for emphasis: it is necessary for uniqueness of solutions and it is essential for
17 numerical stability.

18 While other boundary conditions appear naturally in applications, we consider the
19 simplest boundary conditions: the Dirichlet problem in a convex bounded subset $\Omega \subset \mathbb{R}^d$
20 with boundary $\partial\Omega$,

$$u(x) = g(x), \quad \text{for } x \text{ on } \partial\Omega. \quad (\text{D})$$

21 Under suitable assumptions on the domain and the functions $f(x), g(x)$, recalled in sub-
22 section 2.1, there exist unique classical (C^2) solutions to (MA), (C). However, when
23 these conditions fail, solutions can be singular. For singular solutions, the correct notion
24 of weak solutions must be used. In this case, novel discretizations and solutions methods
25 must be used to approximate the solution.

26 *1.2. Applications*

27 The PDE (MA) is a geometric equation, which goes back to Monge and Ampère
28 (see [1]). The equation naturally arises in geometric problems of existence and uniqueness
29 of surfaces with proscribed metrics or curvatures [2, 3]. Early applications identified
30 in [4] include dynamic meteorology, elasticity, and geometric optics [5, 6, 7, 8]. For an
31 application of Monge-Ampère equations in mathematical finance, see [9].

32 The Monge-Ampère equation arises as the optimality conditions for the problem of
33 optimal mass transport with quadratic cost [1, 10, 11]. This application of the Monge-
34 Ampère equation has been used in many areas: image registration [12, 13, 14], mesh
35 generation [15, 16, 17], reflector design [18], and astrophysics (estimating the shape of
36 the early universe) [19].

37 The problem here is to find a mapping $\mathbf{g}(x)$ that moves the measure $\mu_1(x)$ to $\mu_2(y)$
38 and minimizes the transportation cost functional

$$\int_{\mathbb{R}^d} |x - \mathbf{g}(x)|^2 d\mu_1.$$

39 The optimal mapping is given by $\mathbf{g} = \nabla u$, where u satisfies the Monge-Ampère equation

$$\det(D^2u(x)) = \mu_1(x)/\mu_2(\nabla u(x)).$$

40 In this situation, the Dirichlet boundary condition (D) is replaced by the implicit bound-
41 ary condition

$$\mathbf{g}(\cdot) : \Omega_1 \rightarrow \Omega_2 \quad (1)$$

where the sets Ω_1 and Ω_2 are the support of the measures μ_1, μ_2 . These boundary conditions are difficult to implement numerically; we are not aware of an implementation using PDE methods. For many applications, both domains are squares, and a simplifying assumption that edges are mapped to edges allows Neumann boundary conditions to be used. In other applications, periodic boundary conditions are used.

In other problems, the Monge-Ampère operator appears in an *inequality constraint* in a variational problem for optimal mappings where the cost is no longer the transportation cost. Here the operator has the effect of restricting the local area change on the set of admissible mappings, see [20] or [21].

1.3. Related numerical works

Despite the number of applications, until recently there have been few numerical publications devoted to solving the Monge-Ampère equation. We make a distinction between numerical approaches with optimal transportation type boundary conditions (1) and the standard Dirichlet boundary conditions (D). In the latter case, a number of numerical methods have been recently proposed for the solution of the Monge-Ampère equation.

An early work is [4], which presents a discretization which converges to the Aleksandrov solution in two dimensions. Another early work by Benamou and Brenier [22] used a fluid mechanical approach to compute the solution to the optimal transportation problem.

For the problem with Dirichlet boundary conditions which is treated here, a series of papers have recently appeared by two groups of authors, Dean and Glowinski [23, 24, 25], and Feng and Neilan, [26, 27]. The methods introduced by these authors perform best in the regular case and can break down in the singular case. See [28] a more complete discussion.

We also mention the works [29], in the periodic case, and [15] for applications to mappings. The method of [30] treats the problem of periodic boundary conditions in odd dimensional space.

1.4. Numerical challenges

When the conditions for regularity are satisfied, classical solutions can be approximated successfully using a range of standard techniques (see, for example works such as [23, 24, 25], and [26, 27]). However, for singular solutions, standard numerical methods break down: either by becoming unstable, poorly conditioned, or by selecting the wrong (non-convex) solution.

Weak solutions

For singular solutions, the appropriate notion of weak (viscosity or Aleksandrov) solutions must be used. Numerical methods have been developed which capture weak solutions: Olikar and Prussner, in [4], presents a method which converges to the Aleksandrov solution. One of the authors introduced a finite difference method which converges to the viscosity solution in [31]. Both of these methods were restricted to two dimensions. However, methods which are provably convergent may have lower accuracy or slower solution methods than other methods which are effective for regular solutions. In [32] we introduced a monotone discretization which is valid in arbitrary dimensions. A proof

85 of convergence to viscosity solutions is provided, as well as a proof of convergence of
86 Newton's method.

87 *Convexity*

88 The convexity constraint is necessary for both uniqueness and stability. In partic-
89 ular, the equation (MA) fails to be elliptic if u is non-convex (see subsection 2.5). so
90 instabilities can arise if the convexity condition (C) is violated, as demonstrated in sub-
91 section 8.1. Any approximation of (MA) requires some selection principle to choose the
92 convex solution. This selection principle can be built in to the discretization, as in [31],
93 or built in to the solution method, as in [28].

94 *Accuracy*

95 The convergent monotone schemes of [31] and [32] use a wide stencil, and the accuracy
96 of the scheme depends on the *directional resolution*, which depends on the width of the
97 stencil. As we demonstrate below, for highly singular solutions, such as (17), the direc-
98 tional resolution error can dominate. On the other hand, more accurate discretizations,
99 such as standard finite differences, can be unstable for singular solutions.

100 *Fast solvers*

101 Previous work by the authors and a coauthor [28] investigated fast solvers for (MA).
102 An explicit method was presented which was moderately fast, independent of the solution
103 time. For regular solutions, a faster (by an order of magnitude) semi-implicit solution
104 method was introduced (see subsection 6.2) but this method was slower (by an order of
105 magnitude) on singular solutions.

106 **2. Analysis and weak solutions**

107 In this section we present regularity results and background analysis which inform
108 the numerical approach taken in this work. In particular, the regularity results of sub-
109 section 2.1 are used to determine the discretization used in section 5.

110 The definition of viscosity solutions and Aleksandrov solutions presented in subsec-
111 tion 2.2-2.3 are used to make sense of the weak solutions (15) and (17), respectively.

112 *2.1. Regularity*

113 Under the following conditions, the Monge-Ampère equation is guaranteed to have
114 a unique $C^{2,\alpha}$ solution. Regularity results for the Monge-Ampère equation have been
115 established in [33, 34, 35]. We refer to the book [36] for the following result.

$$\begin{cases} \text{The domain } \Omega \text{ is strictly convex with boundary } \partial\Omega \in C^{2,\alpha}. \\ \text{The boundary values } g \in C^{2,\alpha}(\partial\Omega). \\ \text{The function } f \in C^\alpha(\Omega) \text{ is strictly positive.} \end{cases} \quad (2)$$

116 **Remark 1.** In the extreme case, with $f(x) = 0$ for all $x \in \Omega$, the equation (MA),(C)
117 reduces to the computation of the convex envelope of the boundary conditions [37, 38].
118 In this case, solutions may not even be continuous up to the boundary and can also be
119 non-differentiable in the interior.

120 **Remark 2.** While it is usual to perform numerical solutions on a rectangle, regularity
121 can break down in particular convex polygons [11, 39].

122 2.2. Viscosity solutions

123 We recall the definition of viscosity solutions [40], which are defined for the Monge-
124 Ampère equation in [36].

125 **Definition 1.** Let $u \in C(\Omega)$ be convex and $f \geq 0$ be continuous. The function u is
126 a *viscosity subsolution (supersolution)* of the Monge-Ampère equation in Ω if whenever
127 convex $\phi \in C^2(\Omega)$ and $x_0 \in \Omega$ are such that $(u - \phi)(x) \leq (\geq)(u - \phi)(x_0)$ for all x in a
128 neighbourhood of x_0 , then we must have

$$\det(D^2\phi(x_0)) \geq (\leq)f(x_0).$$

129 The function u is a *viscosity solution* if it is both a viscosity subsolution and supersolution.

130 **Example 1 (Viscosity solution of Monge-Ampère).** We consider an example which
131 will later be solved numerically in two and three dimensions (sections 8-9). Consider (MA)
132 with solution and f given by

$$u(\mathbf{x}) = \frac{1}{2}((|\mathbf{x}| - 1)^+)^2, \quad f(\mathbf{x}) = (1 - 1/|\mathbf{x}|)^+.$$

133 This function, although it is not a classical C^2 solution of the Monge-Ampère equa-
134 tion, is a viscosity solution.

135 2.3. Aleksandrov solutions

136 Next we turn our attention to the Aleksandrov solution, which is a more general weak
137 solution than the viscosity solutions. Here f is generally a measure [36]. We begin by
138 recalling the definition of the normal mapping or subdifferential of a function.

139 **Definition 2.** The *normal mapping (subdifferential)* of a function u is the set-valued
140 function ∂u defined by

$$\partial u(x_0) = \{p : u(x) \geq u(x_0) + p \cdot (x - x_0)\}, \quad \text{for all } x \in \Omega.$$

141 For a set $V \subset \Omega$, we define $\partial u(V) = \bigcup_{x \in V} \partial u(x)$.

142 Now we want to look at a measure generated by the Monge-Ampère operator.

143 **Definition 3.** Given a function $u \in C(\Omega)$, the *Monge-Ampère measure* associated with
144 u is defined as

$$\mu(V) = |\partial u(V)|$$

145 for any set $V \subset \Omega$.

146 This measure naturally leads to the notion of the generalized or Aleksandrov solution
147 of the Monge-Ampère equation.

148 **Definition 4.** Let μ be a Borel measure defined in a convex set $\Omega \in \mathbb{R}^d$. Then the
 149 convex function u is an *Aleksandrov solution* of the Monge-Ampère equation

$$\det(D^2u) = \mu$$

150 if the Monge-Ampère measure associated with u is equal to the given measure μ .

151 **Example 2 (Aleksandrov solution).** As an example, we consider the cone and the
 152 the scaled Dirac measure

$$u(\mathbf{x}) = |\mathbf{x}|, \quad \mu(V) = \pi \int_V \delta(\mathbf{x}) d\mathbf{x}.$$

153 2.4. A PDE for convexity

154 The convexity constraint (C) is necessary for uniqueness, since without it, $-u$ is also
 155 a solution of (MA).

156 For a twice continuously differentiable function u , the convexity restriction (C) can be
 157 written as D^2u is positive definite. Since we wish to work with less regular solutions, (C)
 158 can be enforced by the equation

$$\lambda_1(D^2u) \geq 0,$$

159 understood in the viscosity sense [37, 38], where $\lambda_1[D^2u]$ is the smallest eigenvalue of the
 160 Hessian of u .

161 The convexity constraint can be absorbed into the operator by defining

$$\det^+(M) = \prod_{j=1}^d \lambda_j^+ \tag{3}$$

162 where M is a symmetric matrix, with eigenvalues, $\lambda_1 \leq \dots, \leq \lambda_n$ and

$$x^+ = \max(x, 0).$$

163 Using this notation, (MA),(C) becomes

$$\det^+(D^2u(x)) = f(x), \quad \text{for } x \text{ in } \Omega \tag{MA}^+$$

164 **Remark 3.** Notice that there is a trade off in defining (3): the constraint (C) is elimi-
 165 nated but the operator becomes non-differentiable near singular matrices.

166 2.5. Linearization and ellipticity

167 The linearization of the determinant is given by

$$\nabla \det(M) \cdot N = \text{trace}(M_{adj}N)$$

168 Where M_{adj} is the adjugate [41], which is the transpose of the cofactor matrix. The
 169 adjugate matrix is positive definite if and only if M is positive definite. When the matrix
 170 M is invertible, the adjugate, M_{adj} , satisfies

$$M_{adj} = \det(M)M^{-1} \tag{4}$$

171 We now apply these considerations to the linearization of the Monge-Ampère opera-
 172 tor. When $u \in C^2$ we can linearize this operator as

$$\nabla_M \det(D^2u) \cdot v = \text{trace}((D^2u)_{adj}D^2v). \tag{5}$$

173 **Example 3.** In two dimensions we obtain

$$\nabla_M \det(D^2 u) v = u_{xx} v_{yy} + u_{yy} v_{xx} - 2u_{xy} v_{xy}$$

174 which is homogenous of order one in $D^2 u$. In dimension $d \geq 2$, the linearization is
175 homogeneous order $d - 1$ in $D^2 u$.

176 The linear operator

$$L[u] \equiv \text{trace} A(x) D^2 u$$

177 is *elliptic* if the coefficient matrix $A(x)$ is positive definite.

178 **Lemma 1.** *Let $u \in C^2$. The linearization of the Monge-Ampère operator, (5) is elliptic*
179 *if $D^2 u$ is positive definite or, equivalently, if u is (strictly) convex.*

180 **Remark 4.** When the function u fails to be strictly convex, the linearization can be
181 degenerate elliptic, which affects the conditioning of the linear system (5). When the
182 function u is nonconvex, the linear system can be unstable.

183 The definition of a nonlinear elliptic PDE operator generalizes the definition of linear
184 elliptic operator. It also allows for the operators to be non-differentiable.

185 **Definition 5.** Let the PDE operator $F(M)$ be a continuous function defined on sym-
186 metric matrices. Then $F(M)$ is *elliptic* if it satisfies the monotonicity condition

$$F(M) \leq F(N) \text{ whenever } M \leq N,$$

187 where for symmetric matrices $M \leq N$ means $x^T M x \leq x^T N x$ for all x .

188 **Example 4.** The operator $\det^+(M)$ is a non-decreasing function of the eigenvalues, so
189 it is elliptic.

190 3. The standard finite difference discretization

191 We begin by considering the standard finite difference discretization of the Monge-
192 Ampère equation. For brevity, we describe the discretization in two dimensions, but this
193 is easily generalized to higher dimensions.

194 This discretization does not enforce the convexity condition (C), so it can lead to
195 instabilities. In particular, we show in subsection 8.1 that Newton's method can become
196 unstable if this discretization is used.

197 The Monge-Ampère operator has a particularly simple form in two dimensions:

$$\det(D^2 u) = \frac{\partial^2 u}{\partial x^2} \frac{\partial^2 u}{\partial y^2} - \left(\frac{\partial^2 u}{\partial x \partial y} \right)^2, \quad \text{in } \Omega \subset \mathbb{R}^2.$$

198 In two dimensions, the natural discretization of the operator is given by

$$MA^N[u] \equiv (\mathcal{D}_{xx} u)(\mathcal{D}_{yy} u) - (\mathcal{D}_{xy} u)^2 \quad (MA)^N$$

where, writing h for the spatial resolution of the grid,

$$\begin{aligned} [\mathcal{D}_{xx}u]_{ij} &= \frac{1}{h^2} (u_{i+1,j} + u_{i-1,j} - 2u_{i,j}) \\ [\mathcal{D}_{yy}u]_{ij} &= \frac{1}{h^2} (u_{i,j+1} + u_{i,j-1} - 2u_{i,j}) \\ [\mathcal{D}_{xy}u]_{ij} &= \frac{1}{4h^2} (u_{i+1,j+1} + u_{i-1,j-1} - u_{i-1,j+1} - u_{i+1,j-1}). \end{aligned}$$

Remark 5. There is no reason to assume that the standard discretization converges. In fact, the two dimensional scheme has multiple solutions. In [28] this discretization was used, but the solvers were designed to select the convex solution.

4. Convergent monotone discretization

The method of [31] describes a discretization of the two-dimensional Monge-Ampère equation that converges to the viscosity solution. In [32] we introduced another discretization, which generalized to higher dimensions, and also converged to the viscosity solution. Both methods require the use of a wide stencil scheme, which has an additional discretization parameter, the *directional resolution*, explained below.

In addition to being monotone, which means it is provably convergent, the latter method discretizes the convexified version of the equation, $(MA)^+$, which is enough to ensure convergence of Newton's method. The proof of this result can be found in [32].

In this section we present the convergent discretization, which will be used to build the hybrid solver.

4.1. Wide stencils

When we discretize the operator on a finite difference grid, we approximate the second derivatives by centred finite differences (spatial discretization). In addition, we consider a finite number of possible directions ν that lie on the grid (directional discretization).

We consider the finite difference operator for the second directional derivative in the direction ν , which lies on the finite difference grid. These directional derivatives are discretized by simply using finite differences on the grid

$$\mathcal{D}_{\nu\nu}u_i = \frac{1}{|\nu|h^2} (u(x_i + \nu h) + u(x_i - \nu h) - 2u(x_i)).$$

Depending on the direction of the vector ν , this may involve a wide stencil. At points near the boundary of the domain, some values required by the wide stencil will not be available; see Figure 1. In these cases, we use interpolation at the boundary to construct a (lower accuracy) stencil for the second directional derivative; see [31] for more details.

Since the discretization considers only a finite number of directions ν , there will be an additional term in the consistency error coming from the angular resolution $d\theta$ of the stencil. This angular resolution will decrease and approach zero as the stencil width is increased.

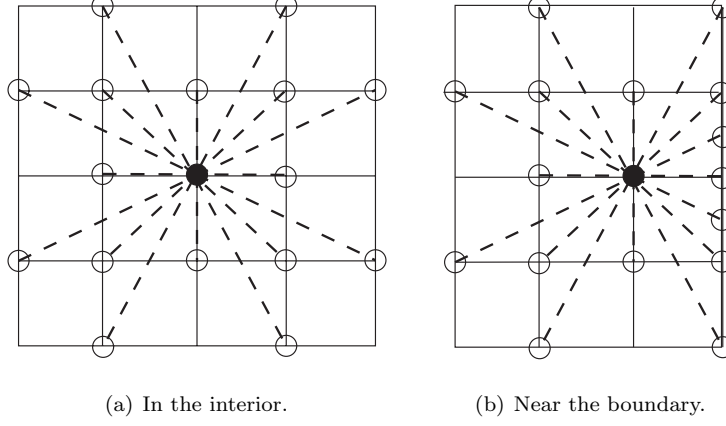


Figure 1: Wide stencils on a two dimensional grid.

228 4.2. Discretization of the convexified Monge-Ampère operator

229 In two dimensions, the largest and smallest eigenvalues of a symmetric matrix can be
 230 represented by the variational formula

$$\lambda_1[A] = \min_{|\nu|=1} \nu^T A \nu, \quad \lambda_2[A] = \max_{|\nu|=1} \nu^T A \nu.$$

231 This formula was used in [31] to build a monotone scheme for the Monge-Ampère oper-
 232 ator, which is the product of the eigenvalues of the Hessian, by replacing the min, max
 233 over all directions, by a finite number of grid directions.

234 In higher dimensions, the formula above does not generalize naturally. Instead, in [32],
 235 we used another characterization, which applied to positive definite matrices.

236 **Lemma 2** (Variational characterization of the determinant). *Let A be a $d \times d$ symmetric*
 237 *positive definite matrix with eigenvalues λ_j and let V be the set of all orthonormal bases*
 238 *of \mathbb{R}^d :*

$$V = \{(\nu_1, \dots, \nu_d) \mid \nu_j \in \mathbb{R}^d, \nu_i \perp \nu_j \text{ if } i \neq j, \|\nu_j\|_2 = 1\}.$$

239 Then the determinant of A is equivalent to

$$\prod_{j=1}^d \lambda_j = \min_{(\nu_1, \dots, \nu_d) \in V} \prod_{j=1}^d \nu_j^T A \nu_j.$$

240 We use Lemma 2 to characterize the determinant of the Hessian of a convex C^2
 241 function ϕ in terms of second directional derivatives of ϕ .

$$\det(D^2\phi) = \min_{(\nu_1, \dots, \nu_d) \in V} \prod_{j=1}^d \nu_j^T D^2\phi \nu_j = \min_{(\nu_1, \dots, \nu_d) \in V} \prod_{j=1}^d \frac{\partial^2 \phi}{\partial \nu_j^2}.$$

242 The convexified Monge-Ampère operator $(MA)^+$ can then be represented by simply
 243 enforcing positivity of the eigenvalues, which leads to the following,

$$\det^+(D^2\phi) = \min_{\{\nu_1 \dots \nu_d\} \in V} \prod_{j=1}^d \left(\frac{\partial^2 \phi}{\partial \nu_j^2} \right)^+.$$

244 To discretize the operator on a finite difference grid, restrict to the set of orthogonal
 245 vectors, \mathcal{G} , available on the given stencil. Then the convexified Monge-Ampère opera-
 246 tor $(MA)^+$ is approximated by

$$MA^M[u] \equiv \min_{\{\nu_1 \dots \nu_d\} \in \mathcal{G}} \prod_{j=1}^d (\mathcal{D}_{\nu_j \nu_j} u)^+ \quad (MA)^M$$

247 **Theorem 3** (Convergence to Viscosity Solution). *Let the PDE (MA) have a unique*
 248 *viscosity solution. Then the solutions of the scheme $(MA)^M$, converges to the viscosity*
 249 *solution of (MA) as $h, d\theta, \delta \rightarrow 0$.*

250 The proof of convergence follows from verifying consistency and degenerate ellipticity
 251 and can be found in [32].

252 5. A hybrid discretization

253 In this section we propose a hybrid discretization of the Monge-Ampère equation
 254 which takes advantage of the best features of each of the previous discretizations. We
 255 want to make use of the natural discretization $(MA)^N$ wherever possible in order to take
 256 advantage of its simplicity and higher accuracy. However, we wish to use the monotone
 257 discretization $(MA)^M$ in regions where the solution may be singular in order to prop-
 258 erly capture the behaviour of the viscosity solution. In this way we hope to achieve the
 259 second-order accuracy of the simple discretization in smooth regions and the monotonic-
 260 ity necessary to capture the behaviour of the viscosity solution in non-smooth regions.

261 We propose the following hybrid scheme.

262 Discretize (MA) using a weighted average of the two discretizations:

$$MA^H = w(x)MA^N + (1 - w(x))MA^M \quad (MA)^H$$

263 where $w : \Omega \rightarrow [0, 1]$ is a weight function defined *a priori* from the data as follows.

264 We first identify Ω^s which is a neighborhood of the possible singular set of u on Ω ,
 265 using conditions (2).

$$\Omega^s = \{x \in \Omega \mid \epsilon < f(x) < 1/\epsilon\} \cup \{x \in \partial\Omega \mid \partial\Omega \text{ flat or } g(x) \notin C^{2,\alpha}\} \quad (6)$$

266 where ϵ is a small parameter, which we can take equal to h , the spatial resolution.

267 Then define $w(x)$ to be a differentiable function which is zero in an h -neighborhood
 268 of Ω^s , and which goes to 1 elsewhere.

269 **Remark 6.** The hybrid scheme will sometimes be less accurate than the standard finite
 270 differences when the solution is C^2 , because it will lose some accuracy at the flat bound-
 271 ary. While this might seem conservative, there are examples, (see [28]), where the flat
 272 boundary causes blow up in the Hessian, so the monotone scheme is needed.

273 6. Explicit and semi-implicit solution methods

274 Any discretization of (MA) leads to a system of nonlinear equations which must be
275 solved in order to obtain the approximate solution.

276 6.1. Explicit solution methods for monotone schemes

277 Using a monotone discretization $F[u]$ of the Monge-Ampère operator, the simplest
278 way to solve the Monge-Ampère equation is by solving the parabolic version of the
279 equation using forward Euler. That is, we perform the iteration

$$u^{n+1} = u^n + dt(F[u^n] - f).$$

280 Explicit iterative methods have the advantage that they are simple to implement, but the
281 number of iterations required suffers from the well known CFL condition (which applies
282 in a nonlinear form to monotone discretizations, as explained in [42]). This approach is
283 slow because for stability it requires a small time step dt , which depends on the spatial
284 resolution h . The time step, which can be computed explicitly, is $\mathcal{O}(h^2)$. This was the
285 approach used in [31].

286 6.2. A semi-implicit solution method

287 The next method we discuss is a semi-implicit method, which involves solving the
288 Laplace equation at each iteration. In [28] we used the identity (8) to build a semi-implicit
289 solution method. We showed that the method is a contraction, but the strictness of the
290 contraction requires strict positivity of f . In practice, this meant that the iteration was
291 fast for regular solutions, but degenerated to become slower than the explicit method
292 when f was zero in large parts of the domain.

293 The conditioning of the linearized equation (5), which affects solution time, depends
294 on the strict convexity of the solution, see lemma 1. The convexity, in turn depends of
295 strict positivity of f , see subsection 2.1. This explains why solution time of the semi-
296 implicit solver depends on regularity.

297 Next, we describe a generalization of the semi-implicit method to higher dimensions.
298 We won't be using the method to solve (MA). Instead, we will use one iteration to set
299 up the initial value for Newton's method.

300 Begin with the following identity for the Laplacian in two dimensions,

$$|\Delta u| = \sqrt{(\Delta u)^2} = \sqrt{u_{xx}^2 + u_{yy}^2 + 2u_{xx}u_{yy}}. \quad (7)$$

So if u solves the Monge-Ampère equation, then

$$|\Delta u| = \sqrt{u_{xx}^2 + u_{yy}^2 + 2u_{xy}^2 + 2f} = \sqrt{|D^2u|^2 + 2f}$$

301 This leads to a semi-implicit scheme for solving the Monge-Ampère equation, used in [28].

$$302 \Delta u^{n+1} = \sqrt{2f + |D^2u^n|^2} \quad (8)$$

To generalize this to \mathbb{R}^d , we can write the Laplacian in terms of the eigenvalues of the Hessian: $\Delta u = \sum_{i=1}^d \lambda_i [D^2 u]$. Taking the d -th power, and expanding, gives the sum of all possible products of d eigenvalues.

$$(\Delta u)^d = d! \prod_{i=1}^d \lambda_i + P(\lambda_1, \dots, \lambda_d),$$

where $P(\lambda)$ is a d -homogeneous polynomial, which we won't need explicitly.

The result is the semi-implicit scheme

$$\Delta u^{n+1} = \sqrt{d! f + P(\lambda_1[D^2 u^n], \dots, \lambda_d[D^2 u^n])}. \quad (9)$$

A natural initial value for the iteration is given by the solution of

$$\Delta u^0 = \sqrt{d! f}. \quad (10)$$

7. Implementation of Newton's method

To solve the discretized equation

$$MA^H[u] = f$$

we use a damped Newton iteration

$$u^{n+1} = u^n - \alpha v^n$$

for some $0 < \alpha < 1$. The damping parameter α is chosen at each step to ensure that the residual $\|MA^H(u^n) - f\|$ is decreasing. (In practice we can often take $\alpha = 1$, but damping is sometimes needed.)

The corrector v^n solves the linear system

$$(\nabla_u MA^H[u^n]) v^n = MA^H[u^n] - f. \quad (11)$$

To set up the equation (11), the Jacobian of the scheme is needed. Since the hybrid discretization is a weighted average of the monotone and standard discretization, and the weight function, $w(x)$, is determined *a priori*, the Jacobian of the hybrid scheme will simply be a weighted average of the corresponding Jacobians.

The Jacobian of the Monge-Ampère operator, discretized using standard finite differences, is given by

$$\nabla_u MA^N[u] = (\mathcal{D}_{xx}u)\mathcal{D}_{yy} + (\mathcal{D}_{yy}u)\mathcal{D}_{xx} - 2(\mathcal{D}_{xy}u)\mathcal{D}_{xy}, \quad (12)$$

which is a discrete version of the linearization of Monge-Ampère (5)

The Jacobian for the monotone discretization is obtained by using Danskin's Theorem [43] and the product rule.

$$\nabla_u MA^M[u] = \sum_{j=1}^d \text{diag} \left(\prod_{k \neq j} \mathcal{D}_{\nu_k^* \nu_k^*} u \right) \mathcal{D}_{\nu_j^* \nu_j^*}$$

where the ν_j^* are the directions active in the minimum in $(MA)^M$.

Thus the corrector is obtained by solving the weighted average of the two linearizations

$$\begin{aligned} (w(x)\nabla_u MA^N[u^n] + (1-w(x))\nabla_u MA^M[u^n])v^n \\ = w(x)MA^N[u^n] + (1-w(x))MA^M[u^n]. \end{aligned} \quad (13)$$

In order for the linear equation (11) to be well-posed, we require the coefficient matrix to be positive definite. As observed in lemma Theorem 1, this condition can fail if the iterate u^n is not strictly convex.

7.1. Initialization of Newton's method

Newton's method requires a good initialization for the iteration. Since we need the resulting linear system to be well posed it is essential that the initial iterate: (i) be convex, (ii) respect the boundary conditions, (iii) be close to the solution.

In order to do this, we first: use one step of the semi-implicit scheme (9), to obtain a close initial value. This amounts to solving (10) along with consistent Dirichlet boundary conditions (D). Then convexify the result, using the method of [37]. Since both the steps can be performed on a very coarse grid, and interpolated onto the finer grid, the cost of the initialization is low.

7.2. Preconditioning

In degenerate examples, the PDE for v^n (13) may be degenerate, which can lead to an ill-conditioned or singular Jacobian. To get around this problem, we regularize the Jacobian to make sure the linear operator is strictly negative definite; this will not change the fixed points of Newton's method. We accomplish this by replacing the second directional derivatives $u_{\nu\nu}$ with

$$\tilde{u}_{\nu\nu} = \max\{u_{\nu\nu}, \epsilon\}$$

Here ϵ is a small parameter. In the computations of section 8, we take $\epsilon = \frac{1}{2dx^2} \times 10^{-8}$.

8. Computational results in two dimensions

In this section, we summarize the results of a number of two-dimensional examples solved using the hybrid scheme described in section 5. In particular, we are interested in comparing the computation time for Newton's method with the time required by the methods proposed in [28]. We also visualize the map generated by the gradient of the solution.

These computations are performed on an $N \times N$ grid on the square $[0, 1]^2$. The monotone scheme used a 17 point stencil.

When needed as part of the initialization, the convex envelope is computed on a coarse grid using the discretization described in [37]. Since the solution can be computed on a coarse grid, and interpolated, the added computational time is negligible.

353 8.1. Failure of Newton's method for natural finite differences

354 In this section, we give an example where Newton's method breaks down when stan-
 355 dard finite differences are used.

356 We chose an example which is only singular at one point, on the boundary. Never-
 357 theless, this mild singularity is enough for Newton's method to break down.

358 Consider the solution of (MA) in $[0, 1]^2$, given by

$$u(\mathbf{x}) = -\sqrt{2 - |\mathbf{x}|^2}, \quad f(\mathbf{x}) = 2(2 - |\mathbf{x}|^2)^{-2}$$

359 The gradient of the solution is unbounded on $|\mathbf{x}| = 2$, in particular at the point $(1, 1)$.
 360 The singularity arises from the fact that f is unbounded there.

361 Due to the singularity, there is an instability in Newton's method if the natural finite
 362 difference method is used. The iteration is initialized with the exact solution. The result
 363 after performing two iterations of Newton's method along with the gradient map, is
 364 illustrated in Figure 2. The correct computed solution is presented in Figure 3(g)-3(h).

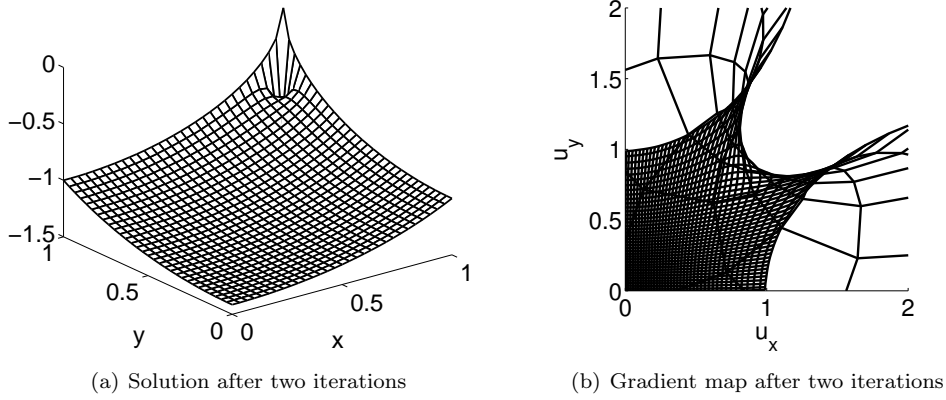


Figure 2: Failure of Newton's method using standard finite differences: the solution oscillates and becomes non-convex.

365 8.2. Four representative examples

366 We have tested the hybrid method on a number of examples of varying regularity;
 367 the results are summarized in subsection 8.4-8.3. To illustrate these results, we present
 368 more detailed results for four representative examples.

369 Write $\mathbf{x} = (x, y)$, and $\mathbf{x}_0 = (.5, .5)$ for the center of the domain.

370 The first example solution, which is smooth and radial, is given by

$$u(\mathbf{x}) = \exp\left(\frac{|\mathbf{x}|^2}{2}\right), \quad f(\mathbf{x}) = (1 + |\mathbf{x}|^2) \exp(|\mathbf{x}|^2). \quad (14)$$

371 The second example, which is C^1 , is given by

$$u(\mathbf{x}) = \frac{1}{2} \left((|\mathbf{x} - \mathbf{x}_0| - 0.2)^+ \right)^2, \quad f(\mathbf{x}) = \left(1 - \frac{0.2}{|\mathbf{x} - \mathbf{x}_0|} \right)^+. \quad (15)$$

372 The third example is the one which was used in subsection 8.1 to demonstrate that
 373 Newton's method for standard finite differences is unstable. The solution is twice differ-
 374 entiable in the interior of the domain, but has an unbounded gradient near the boundary
 375 point $(1, 1)$. The solution is given by

$$u(\mathbf{x}) = -\sqrt{2 - |\mathbf{x}|^2}, \quad f(\mathbf{x}) = 2(2 - |\mathbf{x}|^2)^{-2}. \quad (16)$$

376 This final is example solution is the cone, which was discussed in subsection 2.3. It
 377 is Lipschitz continuous.

$$u(\mathbf{x}) = \sqrt{|\mathbf{x} - \mathbf{x}_0|}, \quad f = \mu = \pi \delta_{\mathbf{x}_0} \quad (17)$$

378 In order to approximate the solution on a grid with spatial resolution h , using viscosity
 379 solutions, we approximate the measure μ by its average over the ball of radius $h/2$, which
 380 gives

$$f^h = \begin{cases} 4/h^2 & \text{for } |\mathbf{x} - \mathbf{x}_0| \leq h/2, \\ 0 & \text{otherwise.} \end{cases}$$

381 8.3. Visualization of solutions and gradient maps

382 In Figure 3 the solutions and the gradient maps for the three representative examples
 383 are presented. For example (17) the gradient map is too singular to illustrate. To
 384 visualize the maps, the image of a Cartesian mesh under the mapping

$$\begin{pmatrix} x \\ y \end{pmatrix} \rightarrow \begin{pmatrix} \mathcal{D}_x u \\ \mathcal{D}_y u \end{pmatrix}$$

385 is shown, where $(\mathcal{D}_x u, \mathcal{D}_y u)$ is the numerical gradient of the solution of the Monge-
 386 Ampère equation. The image of a circle is plotted for visualization purposes, the equation
 387 is solved on a square. For reference, the identity mapping is also displayed.

388 In each case, the maps agree with the maps obtained using the gradient of the exact
 389 solution.

390 8.4. Computation time

391 The computation times for the four representative examples is presented in Table 1.
 392 The computations time are compared to those for the Gauss-Seidel and Poisson iterations
 393 described in [28]. The Newton solver is faster in terms of absolute solution time in each
 394 case. Table 2 presents of order of magnitude solutions times. The order of magnitude
 395 solution time for Newton's method is independent of the regularity of the solutions and
 396 faster than both of the other methods.

397 8.5. Accuracy

398 Numerical errors are presented in Table 3. We compare the accuracy of the hybrid
 399 scheme to the standard finite difference discretization, (using the results of [28]) and to
 400 the monotone scheme which was also solved using Newton's method.

401 We discuss each example in turn.

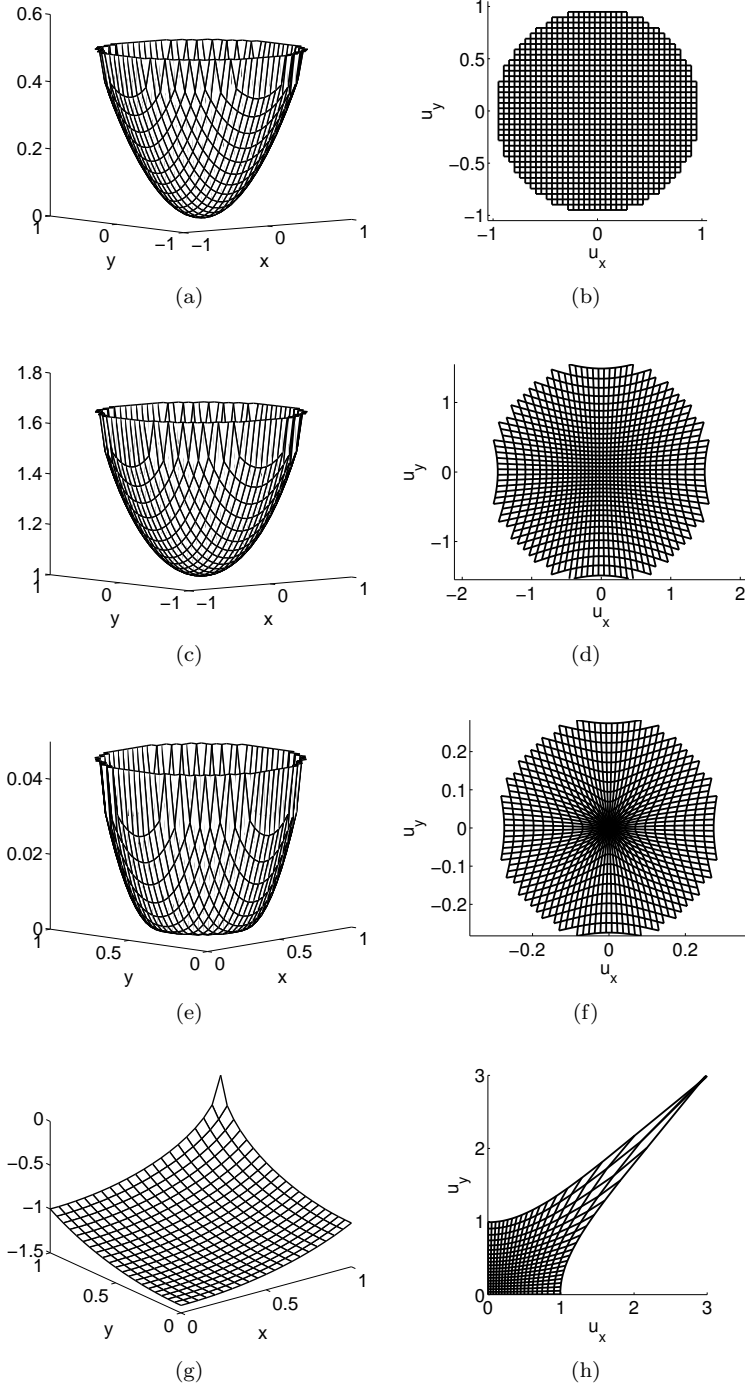


Figure 3: Solutions and mappings for the (a),(b) identity map, (c),(d) C^2 example, (e),(f) C^1 example, and (g),(h) example with blow-up.

C^2 Example (14)				
N	Newton	CPU Time (seconds)		
	Iterations	Newton	Poisson	Gauss-Seidel
31	3	0.2	0.7	2.2
45	4	0.2	1.1	4.1
63	4	0.4	1.9	15.0
89	4	1.0	4.8	57.6
127	5	2.9	9.6	236.7
181	5	9.0	23.2	1004.0
255	5	30.5	52.6	—
361	6	131.4	162.6	—

C^1 Example (15)				
N	Newton	CPU Time (seconds)		
	Iterations	Newton	Poisson	Gauss-Seidel
31	4	0.4	1.1	0.8
45	6	0.4	6.1	2.8
63	7	0.8	20.5	9.5
89	9	2.0	80.0	35.9
127	11	5.7	256.8	145.5
181	13	17.7	—	558.0
255	16	55.3	—	—
361	20	200.0	—	—

Example with blow-up (16)				
N	Newton	CPU Time (seconds)		
	Iterations	Newton	Poisson	Gauss-Seidel
31	4	0.2	0.5	0.8
45	4	0.4	1.4	5.3
63	4	0.7	2.9	19.4
89	5	1.8	8.1	74.1
127	7	5.1	17.7	293.3
181	7	12.9	51.4	1637.1
255	7	36.1	128.2	—
361	8	152.9	374.5	—

$C^{0,1}$ (Lipschitz) Example (17)				
N	Newton	CPU Time (seconds)		
	Iterations	Newton	Poisson	Gauss-Seidel
31	9	0.5	5.3	0.8
45	11	0.6	27.8	5.9
63	15	1.4	91.9	21.5
89	22	4.3	451.0	90.5
127	32	14.1	1758.2	373.9
181	30	34.6	—	1576.1
255	34	101.7	—	—
361	29	280.2	—	—

Table 1: Computation times for the Newton, Poisson, and Gauss-Seidel methods for four representative examples.

Method	Regularity of Solution		
	$C^{2,\alpha}$ (14)	$C^{1,\alpha}$ (15) and (16)	$C^{0,1}$ (17)
Gauss-Seidel	Moderate ($\sim \mathcal{O}(M^{1.8})$)	Moderate ($\sim \mathcal{O}(M^{1.9})$)	Moderate ($\sim \mathcal{O}(M^2)$)
Poisson	Fast ($\sim \mathcal{O}(M^{1.4})$)	Fast-Slow ($\sim \mathcal{O}(M^{1.4})$ –blow-up)	Slow ($\sim \mathcal{O}(M^2)$ –blow-up)
Newton	Fast ($\sim \mathcal{O}(M^{1.3})$)	Fast ($\sim \mathcal{O}(M^{1.3})$)	Fast ($\sim \mathcal{O}(M^{1.3})$)

Table 2: Order of magnitude computation time for the different solvers in terms of the regularity of solutions. Here $M = N^2$ is the total number of grid points.

402 *The C^2 solution (14)*

403 The standard finite difference schemes gives $\mathcal{O}(h^2)$ accuracy (see [28]). In this case,
 404 the hybrid scheme is slightly *less* accurate, because the monotone scheme is used near the
 405 boundary. On a strictly convex domain the hybrid scheme would reduce to the standard
 406 discretization and achieve the same accuracy.

407 The effect diminishes as the number of grid points increases so that the number of
 408 interior points using the higher order scheme dominates. Accuracy approaches $\mathcal{O}(h^2)$ as
 409 the number of grid points increases. This is a definite improvement over the monotone
 410 scheme, which has its accuracy limited by the stencil width.

411 *The C^1 solution (15)*

412 The accuracy is $\mathcal{O}(h)$, which is similar to the standard discretization and better
 413 than the limited accuracy permitted by the monotone discretization with a fixed stencil
 414 width. We also look at the error at each point (see Figure 4); it is evident that the
 415 singularity around the circle is the factor that most affects the accuracy. Because of this
 416 non-smoothness, there is no reason to expect our scheme to produce the $\mathcal{O}(h^2)$ accuracy
 417 that is possible on C^2 solutions.

418 *The blow-up solution (16)*

419 In this case, the hybrid scheme accuracy is $\mathcal{O}(h^{1.5})$. This is better than the accuracy
 420 of both the standard discretization, which was $\mathcal{O}(h^{0.5})$ [28], and the monotone scheme,
 421 which is limited by the stencil width.

422 *The cone solution (17)*

423 For this singular example, the hybrid scheme is identical to the monotone scheme
 424 (since the right-hand side is either 0 or very large everywhere in the domain). Con-
 425 sequently, the angular resolution (stencil width) limits the accuracy of solutions. We
 426 observed that the 17 point stencil reduced the error by an order of magnitude compared
 427 to the 9 point stencil. This dependence on the stencil width is also evident in the surface
 428 plot of error (Figure 4), which demonstrates that error is largest along directions that
 429 are not captured by the stencil. Since this solution is so singular the reduced accuracy
 430 is to be expected.

C^2 Example (14)			
N	Maximum Error		
	Standard	Monotone	Hybrid
31	7.14×10^{-5}	89.09×10^{-5}	24.45×10^{-5}
45	3.39×10^{-5}	60.50×10^{-5}	15.29×10^{-5}
63	1.73×10^{-5}	50.88×10^{-5}	9.06×10^{-5}
89	0.87×10^{-5}	47.51×10^{-5}	5.32×10^{-5}
127	0.43×10^{-5}	45.53×10^{-5}	3.02×10^{-5}
181	0.21×10^{-5}	44.65×10^{-5}	1.61×10^{-5}
255	0.11×10^{-5}	44.22×10^{-5}	0.87×10^{-5}
361	0.05×10^{-5}	44.00×10^{-5}	0.46×10^{-5}

C^1 Example (15)			
N	Maximum Error		
	Standard	Monotone	Hybrid
31	2.6×10^{-4}	17.5×10^{-4}	12.2×10^{-4}
45	1.8×10^{-4}	11.6×10^{-4}	5.9×10^{-4}
63	1.5×10^{-4}	9.8×10^{-4}	4.2×10^{-4}
89	0.9×10^{-4}	8.4×10^{-4}	2.6×10^{-4}
127	0.6×10^{-4}	7.9×10^{-4}	2.0×10^{-4}
181	0.4×10^{-4}	7.4×10^{-4}	1.2×10^{-4}
255	—	7.2×10^{-4}	1.0×10^{-4}
361	—	7.0×10^{-4}	0.7×10^{-4}

Example with blow-up (16)			
N	Maximum Error		
	Standard	Monotone	Hybrid
31	17.15×10^{-3}	1.74×10^{-3}	1.74×10^{-3}
45	14.59×10^{-3}	0.98×10^{-3}	0.98×10^{-3}
63	12.53×10^{-3}	0.59×10^{-3}	0.59×10^{-3}
89	10.67×10^{-3}	0.37×10^{-3}	0.35×10^{-3}
127	9.00×10^{-3}	0.35×10^{-3}	0.20×10^{-3}
181	7.59×10^{-3}	0.34×10^{-3}	0.12×10^{-3}
255	6.42×10^{-3}	0.33×10^{-3}	0.07×10^{-3}
361	5.41×10^{-3}	0.33×10^{-3}	0.04×10^{-3}

$C^{0,1}$ (Lipschitz) Example (17)			
N	Maximum Error		
	Standard	Monotone	Hybrid
31	10×10^{-3}	3×10^{-3}	3×10^{-3}
45	8×10^{-3}	3×10^{-3}	3×10^{-3}
63	6×10^{-3}	3×10^{-3}	3×10^{-3}
89	4×10^{-3}	4×10^{-3}	4×10^{-3}
127	3×10^{-3}	4×10^{-3}	4×10^{-3}
181	2×10^{-3}	4×10^{-3}	4×10^{-3}
255	—	4×10^{-3}	4×10^{-3}
361	—	4×10^{-3}	4×10^{-3}

Table 3: Accuracy for the standard, monotone, and hybrid discretizations for four representative examples.

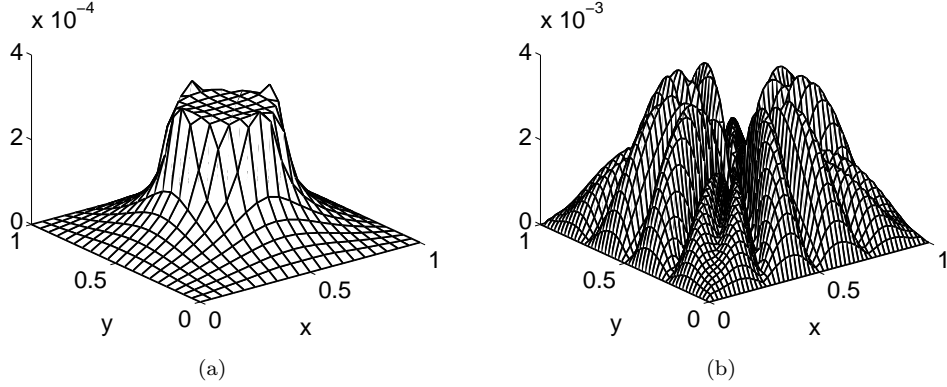


Figure 4: Surface plots of error using the hybrid scheme for the (a) C^1 example and (b) cone example.

9. Computational results in three dimensions.

In this section, we demonstrate the speed and accuracy of the hybrid Newton's method for three dimensional problems. These computations are performed on an $N \times N \times N$ grid on the square $[0, 1]^3$. The monotone scheme used a 19 point stencil.

The size of the computation was restricted by the available memory, not by solution time (the computations were performed on a recent model laptop).

The solution methods of [28] were restricted to the two-dimensional Monge-Ampère equation, so we are no longer able to compare solution times to Newton's method for these examples.

As before, we provide specific results for three representative examples of varying regularity. In this section we use the notation

$$\mathbf{x} = (x, y, z)$$

and let $\mathbf{x}_0 = (.5, .5, .5)$ be the centre of the domain.

The first example is the C^2 solution given by

$$u(\mathbf{x}) = \exp\left(\frac{|\mathbf{x}|^2}{2}\right), \quad f(\mathbf{x}) = (1 + |\mathbf{x}|^2) \exp\left(\frac{3}{2} |\mathbf{x}|^2\right). \quad (18)$$

The second example is the C^1 solution given by

$$u(\mathbf{x}) = \frac{1}{2} ((|\mathbf{x} - \mathbf{x}_0| - 0.2)^+)^2, \quad (19)$$

$$f(\mathbf{x}) = \begin{cases} 1 - \frac{0.4}{|\mathbf{x} - \mathbf{x}_0|} + \frac{0.04}{|\mathbf{x} - \mathbf{x}_0|^2}, & |\mathbf{x} - \mathbf{x}_0| > 0.2 \\ 0 & \text{otherwise.} \end{cases}$$

The third example is the surface of a ball, which is differentiable in the interior of the domain, but has an unbounded gradient at the boundary.

$$u(\mathbf{x}) = -\sqrt{3 - |\mathbf{x}|^2}, \quad f(\mathbf{x}) = 3(3 - |\mathbf{x}|^2)^{-5/2}. \quad (20)$$

448 As indicated by the results in Table 4, the hybrid Newton’s method continues to
 449 perform well in three dimensions. (The fact that the solver required only one iteration
 450 for Example (19) was simply an artifact—for larger problems sizes more iterations were
 451 required.

C^2 Example (18)			
N	Max Error	Iterations	CPU Time (s)
7	0.0151	2	0.04
11	0.0140	3	0.10
15	0.0129	5	0.71
21	0.0121	6	6.72
31	0.0111	5	86.63

C^1 Example (19)			
N	Max Error	Iterations	CPU Time (s)
7	0.0034	1	0.02
11	0.0022	1	0.09
15	0.0016	1	0.22
21	0.0009	1	1.03
31	0.0005	1	17.12

Example with Blow-up (20)			
N	Max Error	Iterations	CPU Time (s)
7	9.6×10^{-3}	1	0.03
11	5.2×10^{-3}	3	0.11
15	4.6×10^{-3}	3	0.48
21	4.0×10^{-3}	6	7.42
31	2.9×10^{-3}	8	138.74

Table 4: Maximum error and computation time for the hybrid Newton’s method on three representative examples.

452 10. Conclusions

453 The purpose of this work was to build a fast, accurate finite difference solver for the
 454 elliptic Monge-Ampère equation.

455 A hybrid finite difference discretization was used which selects between an accurate
 456 standard finite difference discretization and a stable (provably convergent) monotone
 457 discretization. The choice of discretization was based on known regularity results which
 458 depended on the boundary data, g , the right hand side function f , and strict convexity of
 459 the domain. Wherever the requirements on the data are not met, the hybrid discretization
 460 chooses the monotone discretization.

461 The discretized equations were solved by Newton’s method, which is fast, $\mathcal{O}(M^{1.3})$,
 462 where M is the number of data points, independent of the regularity of the solution. The
 463 implementation of Newton’s method was significantly (orders of magnitude) faster than

the two other methods used for comparison. The hybrid discretization was shown to be necessary for stability of Newton's method: an example with a mildly singular solution showed that the standard discretization leads to instabilities.

The hybrid discretization was introduced to improve the accuracy of the monotone discretization on regular solutions. This expected improvement was achieved. On regular solutions the hybrid solver was (asymptotically) as accurate as the standard finite difference discretization. For one moderately singular example the hybrid solver was more accurate than standard finite differences by $\mathcal{O}(h)$.

The discretization and solution method used was not restricted to two dimensions. This allowed for the solution of three dimensional problems on moderate sized grids, with the problem size limited by computer memory, not solution time.

In summary, the solver presented used a novel discretization in general dimensions, accompanied by a fast solution method. The resulting solver is a significant improvement over existing methods for the solution of possibly singular solutions of the elliptic Monge-Ampère equation, in terms of solution time, stability, and accuracy.

References

- [1] L. C. Evans, Partial differential equations and Monge-Kantorovich mass transfer, in: Current developments in mathematics, 1997 (Cambridge, MA), Int. Press, Boston, MA, 1999, pp. 65–126.
- [2] I. Bakelman, Convex analysis and nonlinear geometric elliptic equations, Springer-Verlag, 1994.
- [3] A. V. Pogorelov, Monge-Ampère equations of elliptic type, Translated from the first Russian edition by Leo F. Boron with the assistance of Albert L. Rabenstein and Richard C. Bollinger, P. Noordhoff Ltd., Groningen, 1964.
- [4] V. I. Oliker, L. D. Prussner, On the numerical solution of the equation $(\partial^2 z / \partial x^2)(\partial^2 z / \partial y^2) - (\partial^2 z / \partial x \partial y)^2 = f$ and its discretizations, I, Numer. Math. 54 (1988) 271–293.
- [5] G. J. Haltiner, Numerical weather prediction, Wiley, New York, 1971.
- [6] A. Kasahara, Significance of non-elliptic regions in balanced flows of the tropical atmosphere, Monthly Weather Review 110 (1982).
- [7] J. J. Stoker, Nonlinear elasticity, Gordon and Breach Science Publishers, New York, 1968.
- [8] B. S. Westcott, Shaped reflector antenna design, Research Studies Press, New York, 1983.
- [9] S. D. Stojanovic, Risk premium and fair option prices under stochastic volatility: the hara solution, Comptes Rendus Mathématique 340 (2005) 551 – 556.
- [10] L. Ambrosio, Lecture notes on optimal transport problems, in: Mathematical aspects of evolving interfaces (Funchal, 2000), volume 1812 of *Lecture Notes in Math.*, Springer, Berlin, 2003, pp. 1–52.
- [11] C. Villani, Topics in optimal transportation, volume 58 of *Graduate Studies in Mathematics*, American Mathematical Society, Providence, RI, 2003.
- [12] S. Haker, A. Tannenbaum, R. Kikinis, Mass preserving mappings and image registration, in: MICCAI '01: Proceedings of the 4th International Conference on Medical Image Computing and Computer-Assisted Intervention, Springer-Verlag, London, UK, 2001, pp. 120–127.
- [13] S. Haker, L. Zhu, A. Tannenbaum, S. Angenent, Optimal mass transport for registration and warping, Int. J. Comput. Vision 60 (2004) 225–240.
- [14] T. ur Rehman, E. Haber, G. Pryor, J. Melonakos, A. Tannenbaum, 3D nonrigid registration via optimal mass transport on the GPU, Med Image Anal 13 (2009) 931–40.
- [15] G. L. Delzanno, L. Chacón, J. M. Finn, Y. Chung, G. Lapenta, An optimal robust equidistribution method for two-dimensional grid adaptation based on Monge-Kantorovich optimization, J. Comput. Phys. 227 (2008) 9841–9864.
- [16] J. M. Finn, G. L. Delzanno, L. Chacón, Grid generation and adaptation by Monge-Kantorovich optimization in two and three dimensions, in: Proceedings of the 17th International Meshing Roundtable, pp. 551–568.
- [17] C. J. Budd, J. F. Williams, Moving mesh generation using the parabolic Monge-Ampère equation, SIAM J. Sci. Comput. 31 (2009) 3438–3465.
- [18] T. Glimm, V. Oliker, Optical design of single reflector systems and the Monge-Kantorovich mass

- transfer problem, J. Math. Sci. (N. Y.) 117 (2003) 4096–4108. Nonlinear problems and function theory.
- [19] U. Frisch, S. Matarrese, R. Mohayae, A. Sobolevski, A reconstruction of the initial conditions of the universe by optimal mass transportation, Nature 417 (2002).
- [20] E. Haber, T. Rehman, A. Tannenbaum, An efficient numerical method for the solution of the L^2 optimal mass transfer problem, SIAM J. Sci. Comput. (To Appear.).
- [21] D. Cohen-Or, Space deformations, surface deformations and the opportunities in-between, J. Comput. Sci. Technol 24 (2009) 2–5.
- [22] J.-D. Benamou, Y. Brenier, A computational fluid mechanics solution to the Monge-Kantorovich mass transfer problem, Numer. Math. 84 (2000) 375–393.
- [23] E. J. Dean, R. Glowinski, On the numerical solution of the elliptic Monge-Ampère equation in dimension two: a least-squares approach, in: Partial differential equations, volume 16 of *Comput. Methods Appl. Sci.*, Springer, Dordrecht, 2008, pp. 43–63.
- [24] E. J. Dean, R. Glowinski, An augmented Lagrangian approach to the numerical solution of the Dirichlet problem for the elliptic Monge-Ampère equation in two dimensions, Electron. Trans. Numer. Anal. 22 (2006) 71–96 (electronic).
- [25] R. Glowinski, Numerical methods for fully nonlinear elliptic equations, in: R. Jeltsch, G. Wanner (Eds.), 6th International Congress on Industrial and Applied Mathematics, ICIAM 07, Invited Lectures, pp. 155–192.
- [26] X. Feng, M. Neilan, Mixed finite element methods for the fully nonlinear Monge-Ampère equation based on the vanishing moment method, SIAM J. Numer. Anal. 47 (2009) 1226–1250.
- [27] X. Feng, M. Neilan, Vanishing moment method and moment solutions for fully nonlinear second order partial differential equations, J. Sci. Comput. 38 (2009) 74–98.
- [28] J.-D. Benamou, B. D. Froese, A. M. Oberman, Two numerical methods for the elliptic Monge-Ampère equation, ESAIM: Math. Model. Numer. Anal. 44 (2010).
- [29] G. Loeper, F. Rapetti, Numerical solution of the Monge-Ampère equation by a Newton’s algorithm, C. R. Math. Acad. Sci. Paris 340 (2005) 319–324.
- [30] V. Zheligovsky, O. Podvigina, U. Frisch, The monge-ampère equation: Various forms and numerical solution, J. Comput. Phys. 229 (2010) 5043–5061.
- [31] A. M. Oberman, Wide stencil finite difference schemes for the elliptic Monge-Ampère equation and functions of the eigenvalues of the Hessian, Discrete Contin. Dyn. Syst. Ser. B 10 (2008) 221–238.
- [32] B. D. Froese, A. M. Oberman, Convergent finite difference solvers for viscosity solutions of the Monge-Ampère equation in dimensions two and higher, <http://arxiv.org/abs/1007.0765> (2010).
- [33] L. Caffarelli, L. Nirenberg, J. Spruck, The Dirichlet problem for nonlinear second-order elliptic equations. I. Monge-Ampère equation, Comm. Pure Appl. Math. 37 (1984) 369–402.
- [34] J. I. E. Urbas, The generalized Dirichlet problem for equations of Monge-Ampère type, Ann. Inst. H. Poincaré Anal. Non Linéaire 3 (1986) 209–228.
- [35] L. A. Caffarelli, Interior $W^{2,p}$ estimates for solutions of the Monge-Ampère equation, Ann. of Math. (2) 131 (1990) 135–150.
- [36] C. E. Gutiérrez, The Monge-Ampère equation, Progress in Nonlinear Differential Equations and their Applications, 44, Birkhäuser Boston Inc., Boston, MA, 2001.
- [37] A. M. Oberman, Computing the convex envelope using a nonlinear partial differential equation, Math. Models Methods Appl. Sci. 18 (2008) 759–780.
- [38] A. M. Oberman, L. Silvestre, The Dirichlet problem for the convex envelope, Trans. Amer. Math. Soc. (to appear. <http://arxiv.org/abs/1007.0773>).
- [39] A. V. Pogorelov, The Dirichlet problem for the multidimensional analogue of the Monge-Ampère equation, Dokl. Akad. Nauk SSSR 201 (1971) 790–793.
- [40] M. G. Crandall, H. Ishii, P.-L. Lions, User’s guide to viscosity solutions of second order partial differential equations, Bull. Amer. Math. Soc. (N.S.) 27 (1992) 1–67.
- [41] G. Strang, Linear algebra and its applications, Academic Press [Harcourt Brace Jovanovich Publishers], New York, second edition, 1980.
- [42] A. M. Oberman, Convergent difference schemes for degenerate elliptic and parabolic equations: Hamilton-Jacobi equations and free boundary problems, SIAM J. Numer. Anal. 44 (2006) 879–895 (electronic).
- [43] D. P. Bertsekas, Convex analysis and optimization, Athena Scientific, Belmont, MA, 2003. With Angelia Nedić and Asuman E. Ozdaglar.